

COMPRA: A COMPact Reactive Autonomy framework for subterranean MAV based search-and-rescue operations

Björn Lindqvist¹ · Christoforos Kanellakis¹ ·
Sina Sharif Mansouri¹ · Ali-akbar
Agha-mohammadi² · George Nikolakopoulos¹

Received: 2021-08-17 / Accepted: date

Abstract This work establishes COMPRA, a compact and reactive autonomy framework for fast deployment of Micro Aerial Vehicles (MAVs) in subterranean Search-and-Rescue missions. A COMPRA-enabled MAV is able to autonomously explore previously unknown areas while specific mission criteria are considered e.g. an object of interest is identified and localized, the remaining useful battery life, the overall desired exploration mission duration. The proposed architecture follows a low-complexity algorithmic design to facilitate fully on-board computations, including nonlinear control, state-estimation, navigation, exploration behavior and object localization capabilities. The framework is mainly structured around a reactive local avoidance planner, based on enhanced Potential Field concepts and using instantaneous 3D pointclouds, as well as a computationally efficient heading regulation technique, based on contour detection on an instantaneous camera stream. Those techniques decouple the collision-free path generation from the dependency of a global map and are capable of handling imprecise localization occasions. Field experimental verification of the overall architecture is performed in relevant unknown Global Positioning System (GPS)-denied environments.

Keywords MAV SubT exploration framework · Search-and-rescue Robotics · NMPC · Obstacle Avoidance · MAV autonomy · Object localization

Björn Lindqvist
E-mail: bjorn.lindqvist@ltu.se

Christoforos Kanellakis
E-mail: christoforos.kanellakis@ltu.se

Sina Sharif Mansouri
E-mail: sina.sharif.mansouri@ltu.se

Ali-akbar Agha-mohammadi
E-mail: aliakbar.aghamohammadi@jpl.nasa.gov

George Nikolakopoulos
E-mail: george.nikolakopoulos@ltu.se

¹ The authors are with the Robotics and Artificial Intelligence Team, Department of Computer, Electrical and Space Engineering, Luleå University of Technology, Luleå SE-97187, Sweden. ·

²The author is with Jet Propulsion Laboratory California Institute of Technology Pasadena, CA, 91109.

1 Introduction and Background

In recent years, aerial robotics research has experienced a rapid growth in different applications. Among the major objectives pursued, the overall aim is to increase the corresponding operating autonomy levels, envisioning the development and field deployment of aerial robotic workers capable to explore, inspect and operate in challenging environments without human intervention. In general, Micro Aerial Vehicles (MAVs) have undoubtedly shown powerful merits, as an outcome of their outstanding flying capabilities, in fully controlled and well-defined laboratory environments [1], thus motivating the necessity to integrate such capabilities in real-life field applications. The envisioned use cases that are suitable for such aerial robotics operations, include disaster management missions [2], infrastructure inspection and maintenance [3], subterranean area exploration [4] and more. Focusing in search and rescue missions in subterranean environments, MAVs can provide access to unreachable, complex, dark and dangerous locations, while providing a valuable situational and environmental awareness to the first responders [5]. Autonomous aerial robots can navigate in fully unknown and harsh environments and perform their instructed tasks, without the need of retaining a line of sight to the operator. In this approach, the human exposure to dangerous environments (e.g. blind openings, areas after blasting, etc.) will be significantly minimized, while at the same time will increase the effectiveness of the overall mission. Usually, in this type of environments, there is a lack of natural illumination, there exist unconditioned narrow passages and intersecting paths, dirt, high moisture and dust, which are factors making the environment harsh, complex and challenging for full autonomous missions.

The context of aerial robots in search and rescue missions, requires innovative and applicable in the field solutions that allow for a fast exploration of unknown areas, agile and collision free motion, as well as artifact detection and localization, all consisting of mission attributes that add resilience and robustness in these challenging missions. The focus of this work is the establishment of the COMPRA framework, especially designed for MAVs, including self-localization, Nonlinear Model Predictive Control (NMPC) control, obstacle avoidance, object localization and basic mission behaviour capabilities. A framework that has been extensively developed as part of the NEBULA autonomy [6] for mission oriented drones in SubT environments and as an extension and differentiation from other co-existing complete frameworks for search and rescue operations.

1.1 Related Works

Within the related literature of full exploration mission frameworks in aerial robotics, there have been recently reported a number of works on methodologies for MAV deployment in subterranean environments. In [7] an autonomy framework for object search in underground areas has been proposed. The developed platform utilized onboard visual, thermal and 3D lidar sensors to address a multi-modal localization and mapping scheme. A bifurcated exploration planner is employed with local and global variants to explore the local surroundings of the platform, as well as to relocate the platform in globally defined unexplored paths or return to home. divided in local and global parts. The objects of interest are detected from a Convolutional Neural Network (CNN) detector and localized using ray-casting in an occupancy map combined with binary Bayes filter to avoid erroneous measurements. Similarly, the authors in [8]

developed a MAV system for navigation in constrained tunnel-like environments. The main concept in this work, relies on a model based control scheme that relaxed the tracking performance to handle errors induced by the localization system. Moreover, an A* planning approach on 2D occupancy maps is used for both global navigation and local exploration, while the objects of interest are detected using a CNN and localized by an intersecting 3D rays from a camera projection model with wall and ground modeled by lidar sensors. The detected object can be reported to the DataBase either by following a return trajectory or through a designed mesh network when exploring deepest parts. In [9], a framework for automated MAV motion planning under target location uncertainty in cluttered areas, has been presented in simulation and lab environments. In this work, the navigation problem is modelled as a Partially Observable Markov Decision Process (POMDP) and solved in real time through the Augmented Belief Trees (ABT) algorithm. Additionally, the developed system is able to handle a target detection uncertainty related to false positive detections by using the detection confidence in the POMDP formulation. In [10], the estimation, navigation, mapping and control capabilities for autonomous inspection of penstocks and tunnels using aerial vehicles has been studied, using IMU, cameras and lidar sensors. In [11] the authors present an aerial scout robot for fast navigation in underground tunnels. The developed system enables a resource constrained robot to navigate as a floating object, combining a velocity controller on the x , y and altitude control on the body frame axis, while proposing two different approaches for regulating the heading along the tunnel using either the geometric processing of 2D Lidar scans or Deep Learning classification using monocular camera.

Compared to the State-of-the-Art works [7]-[11] the COMPRA architecture proposes an alternative strategy of the overall mission and the utilized modules related to localization, obstacle avoidance, exploration and object localization, while focusing in a low complexity implementation, as well as developing critical components to be independent of localization or occupancy mapping issues, including the reactive navigation based on Potential Fields obstacle avoidance, as well as the heading regulation. Moreover, the COMPRA core concept relies on the idea that smaller scaled MAVs for narrow passage navigation, have limited flight time and in some application scenarios the higher priority is the fast deployment, compared to complete and detailed coverage of the environments. Table 1 summarizes the modules from all frameworks, depicting the alternative approaches to address the search and rescue mission.

1.2 Contributions

With respect to the related State-of-the-Art, this article describes an autonomy framework for MAVs operated in subterranean locations for search and rescue tasks. The main contributions of our work are listed as follows:

- We present a complete, compact and low complexity system for fast deployment MAVs with baseline capabilities for exploration, NMPC position control, 3D lidar-inertial localization, obstacle avoidance, CNN based object and depth based object localization and return-to-home behaviour.
- We structure the system around a potential field local avoidance architecture, based on instantaneous 3D pointclouds with a key element to handle localization inaccuracies and a vision based heading regulation scheme. More specifically, the avoidance planner is reactive with low computation demands and operates independently

Frameworks	Control	Localization	Obstacle Avoidance	Navigation	Return to Base	Object Detection & Localization	Field Evaluation
[7]	Model Predictive Control [12]	Visual-Thermal-Inertial Odometry [13, 14] fused with Lidar Odometry	global-local graph-based planners [15]	local sampling-based rapidly exploring random graph search planner	global sampling-based rapidly exploring random graph search planner	Yolov3 & Raycasting	underground tunnel
[8]	Model Predictive Control & Acceleration tracking SO(3) controller	2D Lidar odometry (Hector SLAM [16])	modified A* on 2D occupancy map	modified A* on 2D occupancy map	modified A* on 2D occupancy grid	YoloV8000 & Raycasting	underground tunnel
[9]	MAVRKS position control [17]	Realsense T265-Aliumet	occupancy map (offline)	POMDP decision making using actions, states and observations	-	MobileNet SSD & camera footprint with observation belief	lab
[10]	Non Linear tracking control on SE(3) [18, 19]	range and vision-based odometry fused with Unscented Kalman Filter	user high-level waypoint commands	user high-level waypoint commands & local mapper parametric representation on 3D pointclouds	-	-	underground tunnel
[11]	Velocity and altitude tracking NMPC	OpticalFlow-Aliumet-IMU	2D potential fields [20]	velocity based carot-clashing & tunnel risk detection on 3D pointclouds	tunnel risk eval. RGB-D relation & velocity based carot-clashing	-	underground tunnel
COMFRA	Reference tracking NMPC [21, 22]	3D Lidar-Inertial odometry (LIO-SAM [23])	3D potential fields with force normalization and saturation	Position based carot-clashing & image contour open space heading alignment [24]	broaderump following on global waypoints	Yolov4-tiny & Depth Images	underground tunnel

Table 1: MAV autonomy frameworks comparison

from the localization and mapping modules, thus its performance is not directly affected from localization errors. The attractive and repulsive forces have undergone a force-normalization and saturation process to keep smooth and stable performance. Tunnel navigation is challenging, since the MAV has to identify the direction of the flight in unknown areas, while avoiding the surrounding walls. The exploration behaviour incorporates a heading regulation that identifies open spaces in tunnels and generates heading commands to align with the tunnel axis.

- we present extensive experimental verification of the overall architecture in relevant environments to showcase the feasibility and performance of the proposed framework in complete field missions. Comparison with the identified similar mission frameworks cannot be performed due to the lack of complete software open source packages that would allow such action, however insights and highlights on the different point of view have been provided.

The rest of the article is structured as follows. Initially, Section 2 presents detailed information of the COMPRA autonomy stack, while discussing both the baseline navigation framework, as well as the capabilities related to the mission definition. The experimental evaluation of the framework and the corresponding results are presented in Section 3. Finally, Section 4 concludes the article by summarizing the findings.

2 COMPRA Autonomy

2.1 Frame Notation

The world frame \mathcal{W} is fixed with the unit vectors $\{x^{\mathcal{W}}, y^{\mathcal{W}}, z^{\mathcal{W}}\}$ following the East-North-Up (ENU) frame convention. The body frame of the aerial vehicle \mathcal{B} is attached on its base with the unit vectors $\{x^{\mathcal{B}}, y^{\mathcal{B}}, z^{\mathcal{B}}\}$, representing the rotated global coordinates \mathcal{W} in along the z -axis. The $z^{\mathcal{B}}$ is antiparallel to the gravity vector, $x^{\mathcal{B}}$ is looking forward the platform's base and $y^{\mathcal{B}}$ is in the ENU convention. The onboard camera frame \mathcal{C} has unit vectors $\{x^{\mathcal{C}}, y^{\mathcal{C}}, z^{\mathcal{C}}\}$. Furthermore, $y^{\mathcal{C}}$ is parallel to the gravity vector and $z^{\mathcal{C}}$ points in front of the camera. The image plane is defined as \mathcal{I} with unit vectors $[x^{\mathcal{I}}, y^{\mathcal{I}}]$. Figure 1 depicts the utilized main coordinate frames of the aerial platform.

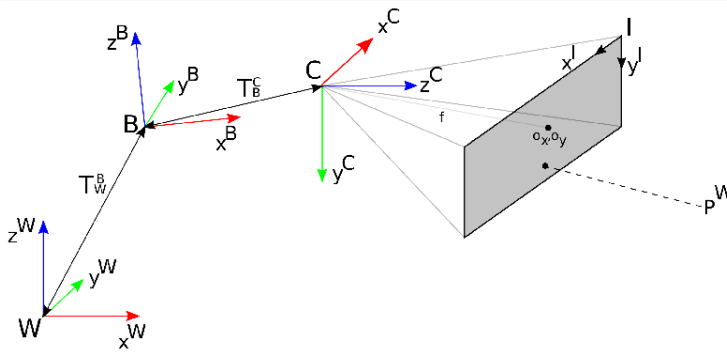


Fig. 1: Coordinate frames, where \mathcal{W} , \mathcal{B} , \mathcal{C} and \mathcal{I} denote world, body, Lidar, camera and image coordinate frames respectively.

2.2 Navigation Framework

In this part we present the fundamental systems to enable the autonomous flight of a MAV along tunnels by using onboard computation unit and sensors. The baseline functionality for the aerial platform is to accomplish an exploration task in unknown underground areas to localize objects of interest. To this end, the COMPRA framework incorporates state estimation, control, avoidance, exploration and object detection and localization capabilities. Initially, it localizes itself in a globally defined coordinate frame combining information of a fiducial based gate calibration scheme with the Lidar-Inertial based state estimation just before the mission starts. The obstacle avoidance scheme is based on Artificial Potential Fields and generates collision-free waypoints. The reactive exploration behaviour guides the MAV along the tunneling environment, while, the control reference tracker uses the information from the other components to provide low level commands for the flight control unit. In the proposed system a single beam lidar facing towards the ground provides altitude measurements relative to the ground $p_z^{\mathbb{L}}$, which are used from other COMPRA subsystems. Figure 2 summarizes COMPRA exploration framework.

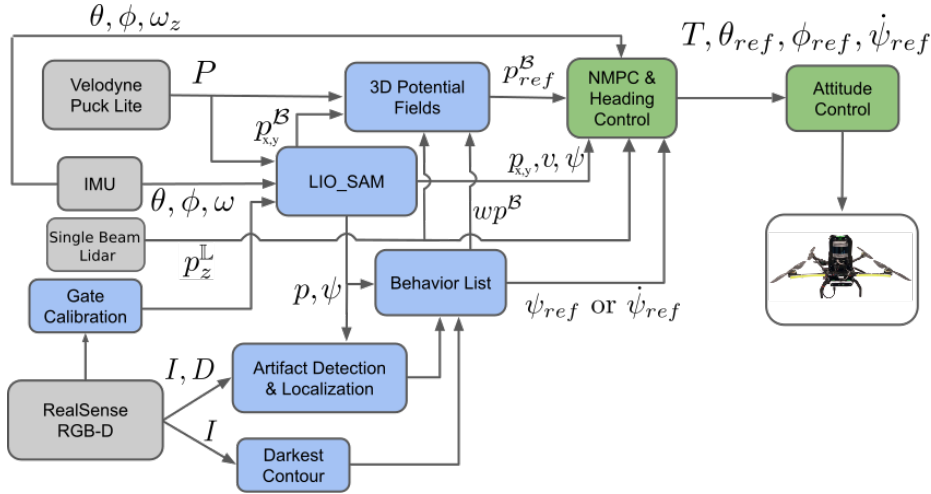


Fig. 2: Overall COMPRA architecture and information flow. On-board sensors are shown in gray, sub-modules/algorithms in blue, and controllers in green.

2.2.1 State-Estimation

The autonomous flight of a MAV requires state-estimation information that is accurate and with low-latency. Generally, research on robot localization, has been and, continues to be a quest, with the aim to establish robotics into everyday life usage. Multiple sensing modules can be used to provide state-estimation information including monocular/depth/stereo/event/thermal cameras, 2D/3D Lidars, Radars, Global Positioning System (GPS), Ultra-Wide Band (UWB) and other, depending on the application needs. In this framework the State-of-the-Art tightly coupled 3D Lidar-Inertial odometry

estimation scheme proposed in [23] is used that provides the resulting state vector $X = [x, y, z, v_x, v_y, v_z, \phi, \theta, \psi, \omega_x, \omega_y, \omega_z]^\top$.

2.2.2 Reference Tracking Controller

While there are a wide range of possible reference tracking controllers for MAVs we use a NMPC. The main benefits of NMPC are the ability to handle constraints, the flexibility in defining the cost function, and that it is directly based on a nonlinear dynamic model of the system. The proposed NMPC is similar in structure to previous papers [21], [22], and as such we will not go into details. The MAV nonlinear model considers eight states namely $x = [p, v, \phi, \theta]$, and as such it is in a yaw-compensated coordinate frame, and thus operates in the UAV body frame. The generated control commands are $u = [T, \theta_{ref}, \phi_{ref}]$ with $\phi_{ref} \in \mathbb{R}$, $\theta_{ref} \in \mathbb{R}$ and $T_{ref} \geq 0$ to be the references in roll, pitch and total mass-less thrust generated by the four rotors, which are very commonly accepted commands, together with a yaw-rate command as $\dot{\psi}_{ref}$, for low level attitude controllers, such as Pixhawk or ROSflight, with T_{ref} commonly mapped to a control signal as $u_t \in [0, 1]$. The yaw angle ψ is controlled with a decoupled simple PD controller. Let $x_{k+j|k}$ denote the predicted state at time step $k+j$, produced at the time step k (and similarly the control action as $u_{k+j|k}$), and N the prediction horizon. We formulate the cost functions to make each state reach the prescribed set-points, while delivering smooth control signals as:

$$J(x_k, u_k; u_{k-1|k}) = \underbrace{\sum_{j=0}^N \|x_{ref} - x_{k+j|k}\|_{Q_x}^2}_{\text{State cost}} \quad (1)$$

$$+ \underbrace{\|u_{ref} - u_{k+j|k}\|_{Q_u}^2}_{\text{Input cost}} + \underbrace{\|u_{k+j|k} - u_{k+j-1|k}\|_{Q_{\Delta u}}^2}_{\text{Input change cost}},$$

where $Q_x \in \mathbb{R}^{8 \times 8}$, $Q_u, Q_{\Delta u} \in \mathbb{R}^{3 \times 3}$ are symmetric positive definite weight matrices for the states, inputs and input rates respectively. Importantly we can directly penalize the change in inputs from one time step to the next by the *input change cost*, promoting non-aggressive control actions. Additionally let us define constraints on the inputs as $u_{min} \leq u_{k+j|k} \leq u_{max}$ and constraints on the change in control inputs, to further enforce smooth control actions, as:

$$|\phi_{ref, k+j-1|k} - \phi_{ref, k+j|k}| \leq \Delta\phi_{max}, \quad (2a)$$

$$|\theta_{ref, k+j-1|k} - \theta_{ref, k+j|k}| \leq \Delta\theta_{max}. \quad (2b)$$

where $\Delta\phi_{max}$ and $\Delta\theta_{max}$ denote the maximum allowed change in roll and pitch references from one time step to the next. The optimization problem to minimize the cost function $J(x_k, u_k; u_{k-1|k})$, while subject to the constraints is solved by the Optimization Engine[25], an open-source and Rust-based parametric optimization software, which is very fast for this type of application. While the input constraints are considered as hard bounds, OpEn utilizes a penalty method[26] to solve for trajectories that satisfy the input rate constraints. The NMPC runs at 20Hz, which is following common inner/outer loop dynamics with the attitude controller running at 100Hz. The prediction horizon N that is considered in the optimization is 20, implying a one second prediction.

2.2.3 Obstacle Avoidance

There are a number of requirements that we pose on the local avoidance scheme, such as to: 1) be reactive e.g. have low computation and latency, 2) be independent of localization and mapping as to prevent crashes due to localization or occupancy-mapping failure, 3) result in smooth and stable behavior of the MAV in any avoidance situation, 4) work directly with the 3D point cloud (again to prevent failures due to drifts or malfunctions in other software). Towards these requirements we propose an Artificial Potential Field formulation with a focus placed on generating a resulting force in the local MAV frame that does not cause oscillations or erratic behavior of the MAV. This is achieved by choosing a potential function (or rather directly a force function) that is continuous and smooth in the area of influence of the potential field, placing saturation limits on the repulsive forces and the change in repulsive forces, and performing force-normalization, as to always generate forces of the same magnitude (which a reference-tracking controller then can be optimally tuned to follow).

Let us denote the local point cloud generated by the 3D lidar as $\{P\}$, where each point is described by a relative position to the lidar frame as $\rho = [\rho_x, \rho_y, \rho_z]$. Let us also denote the repulsive force as $F^r = [F_x^r, F_y^r, F_z^r]$, the attractive force as $F^a = [F_x^a, F_y^a, F_z^a]$, the radius of influence of the potential field as r_F . As we are only interested in points inside the radius of influence, when considering the repulsive force, let's denote the list of such points $\rho_r \in \{P\}$ where $\|\rho_r^i\| \leq r_F$ and $i = 0, 1, \dots, N_{\rho_r}$ (and as such N_{ρ_r} is the number of points to be considered for the repulsive force). Taking inspiration from the classical repulsive force function proposed by Warren [27] we define the repulsive force as:

$$F^r = \sum_{i=0}^{N_{\rho_r}} L \left(1 - \frac{\|\rho_r^i\|}{r_F}\right)^2 \frac{-\rho_r^i}{\|\rho_r^i\|} \quad (3)$$

where L is the repulsive constant and represents the largest possible force-per-point inside r_F . It should also be noted that computing the total force as the sum of multiple smaller "forces" from each point inside r_F also makes the framework more resilient to dust as each individual dust particle does not majorly affect the total force.

Based on the COMPRA framework, we simply denote the attractive force as the next way-point, $wp = [wp_x, wp_y, wp_z]$ generated by the navigation in the local frame, such that $F^a = wp^B - \hat{p}^B$. From an intuitive point of view this can be seen as the attractive force being the vector from the current position to the next given way-point with an unitary gain, while the repulsive force is the shift in the next way-point required to avoid obstacles. Generally, the attractive and repulsive forces are summed to get the total resulting force F . But, since the requirement of a stable and smooth flight is as high for a MAV as with multiple other modules (localization etc.) running from on-board sensors, we propose a force-normalization and saturation on the forces, and on the change in the repulsive force. Let k denote the current sampled time instant and $(k-1)$ the previous sampled time instant. This process is explained in Algorithm 1, with F_{max} and ΔF_{max} being the saturation value and rate-saturation of the repulsive force and $sgn()$ denoting the sign function. The reference position, passed to the reference tracking controller (in the MAV body frame), with included obstacle avoidance, then becomes $p_{ref}^B = F + \hat{p}^B$, where p_{ref}^B are the first three elements of x_{ref} . A separate field evaluation of the potential field algorithm is presented in section 3.2.1, in a relevant dusty subterranean field experimentation area.

Algorithm 1: Force calculation

Inputs: F^a, F_k^r, F_{k-1}^r
if $\|F_k^r\| > F_{max}$ **then**
 $F_k^r \leftarrow \text{sgn}(F_k^r) F_{max}$
if $\|F_k - F_{k-1}\| > \Delta F_{max}$ **then**
 $F_k^r \leftarrow F_{k-1}^r + \text{sgn}(F_k^r - F_{k-1}^r) \Delta F_{max}$
if $\|F^a\| > 1$ **then**
 $F^a \leftarrow \frac{F^a}{\|F^a\|}$
 $F \leftarrow F_k^r + F^a$
if $\|F\| > 1$ **then**
 $F \leftarrow \frac{F}{\|F\|}$
Output: F

2.2.4 Reactive Exploration

The exploration behaviour in this work considers the generation of local reference waypoints $p_{ref}^{\mathcal{B}}$ in 3D, as well as local yaw references ψ_{ref} .

The exploration waypoints follow the heuristic concept of constant value “carrot” chasing in the bodyframe x -axis of the platform. More specifically, the generated waypoints $p_{ref}^{\mathcal{B}}$ always add a constant value ahead of the x -axis, while the motion in y -axis in \mathcal{B} frame depends on the potential fields input, as well as the open space heading control. The waypoints are defined as $wp^{\mathcal{B}} = [p_x^{\mathcal{B}} + 1, p_y^{\mathcal{B}}, p_z^m]$. The local altitude reference p_z^m (or the mission altitude) is kept constant and selected before the mission starts, and the measured local z -position is defined by the range measurements, R_{sbl} , from the single-beam lidar as $p_z^{\mathcal{L}} = R_{sbl} \cos \theta \cos \phi$, e.g. the distance to the ground.

Heading regulation using Darkness Contours Detection Part of the fast deployment and exploration approach of COMPRA is the alignment of the aerial platform heading along the tunnel axis. The baseline approach, employed in this work, integrates the preliminary work [24]. The method initially binarizes the onboard RGB camera stream I by using the Otsu threshold [28] and then calculates the boundaries of the darkest area by using the Moore-Neighbor contour tracking [29], under the assumption that darker areas are located in greater depths. More specifically, it takes advantage of the geometry of the underground tunnel areas, as well as their lack of natural illumination, while it combines them with the onboard illumination of the MAV that keeps track of the tunnel darkest point locally and instantaneously. In the sequel, it initially extracts the darkest areas center, coordinated $\hat{u} = [x^{\mathcal{I}}, y^{\mathcal{I}}]$, which are linearly mapped to $\bar{u} \in [0, 1]$. Finally, the coordinates are converted with respect to the image center coordinates, to the heading rate output $\dot{\psi}_{ref} \in [-0.3 \ 0.3]$ rad/sec that is used only in the first exploration part in the behavior list module 2.3.2 and not in the breadcrumb following return to base navigation part. Figure 3 depicts a visualization of the algorithm.

2.3 Mission Definition

For the overall mission definition of search and rescue in SubT environments, two components must be added to the core COMPRA autonomy kit to fulfill the mission, namely: the object detection and localization based on an image stream from onboard

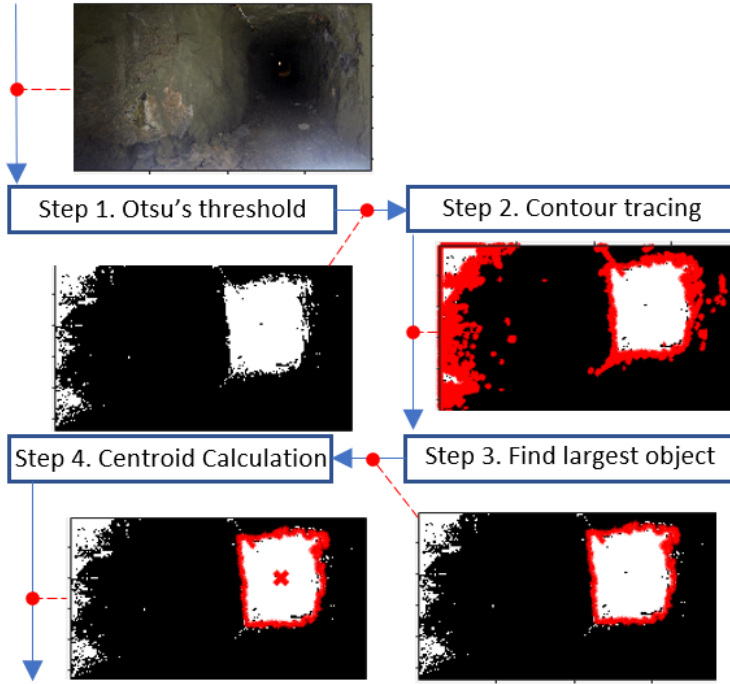


Fig. 3: Illustration of the processing steps for the deepest tunnel point search in the onboard images

cameras, as well as a behavior list for mission execution, that includes returning to base after mission completion.

2.3.1 Object Detection and Localization

In this Section we consider the capability to detect and localize objects of interest with the flying platform, while the overall capability processes visual and depth sensor measurements. The visual detection part is based on the tiny and Intel hardware optimized version [30] of the state of the art CNN object detector Yolo V4 [31]. We trained the network to detect and classify 6 classes defined by the SubT competition using a custom dataset consisting of approximately 700 images for each class. The input size of the images is 416×416 and the output of the algorithm is the detected bounding boxes and the class probability.

The other component of the pipeline is the object localizer, which receives the bounding box measurements from the RGB image stream I . The localizer transfers the identified bounding box in the aligned depth image stream D and extracts the relative position of the object compared to the flying platform in the camera frame \mathcal{C} , defined as $p_{object}^{\mathcal{C}} = [p_x^{\mathcal{C}}, p_y^{\mathcal{C}}, p_z^{\mathcal{C}}]$. Finally the object location is converted in the global world frame \mathcal{W} , defined as $p_{object}^{\mathcal{W}}$, using the transformation $p_{object}^{\mathcal{W}} = {}^{\mathcal{W}}T_{\mathcal{C}} p_{object}^{\mathcal{C}}$, where ${}^{\mathcal{W}}T_{\mathcal{C}}$ denotes the transformation matrix from \mathcal{C} to \mathcal{W} , defined as ${}^{\mathcal{W}}T_{\mathcal{C}} = [R|t]$. The object localizer waits for the input from the detector and once the first object above a specific probability is detected it waits a specific amount of time to

collect more detections and take the mean value. The localizer returns a list $\mathbb{OL} = \{\vec{0}_{3 \times 1}, p_{object1}^{\mathcal{W}}, p_{object2}^{\mathcal{W}}, \dots, p_{objectn}^{\mathcal{W}}\}$, where n is the number of detected objects with $n \in \mathbb{N}_0$. Figure 4 presents the overall architecture on the strategy related to the object detection and localization.

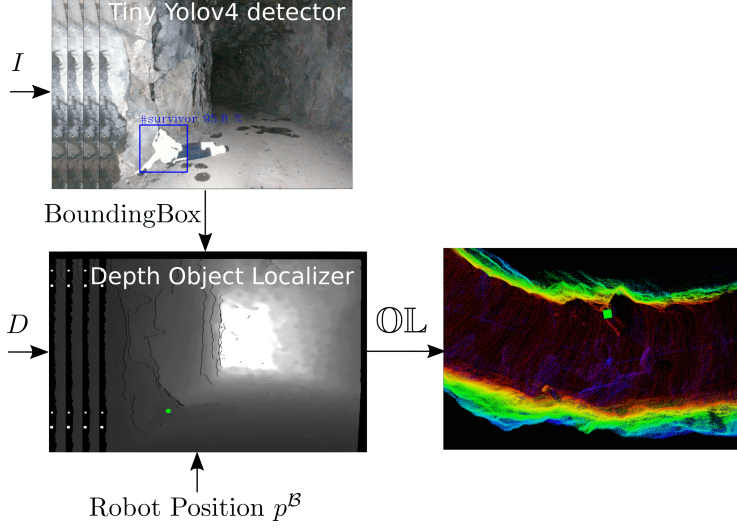


Fig. 4: The object detection and localization pipeline.

2.3.2 Behavior List

The mission behavior of COMPRA is presented in Algorithm 2

On top of all sequences presented in Algorithm 2, the system incorporates a STOP behavior which directly lands the platform on the ground, using either RC switch or a software safety command from the task supervisor. The pre-flight checks include bringup of hardware and all software COMPRA stack. The Breadcrumb Waypoint List \mathbb{BW} is populated with exploration waypoints wp^B at a user desired sampling rate. On the return path, the visited breadcrumb waypoints within a radius are removed from \mathbb{BW} . $T_{mission}^{current}$ and $T_{mission}^{reference}$ refer to current mission time and overall mission time respectively. For the return of the MAV to the mission's starting point, previously visited points are considered in \mathbb{BW} . In this case the MAV, navigates through already mapped areas, which allows relocalization or loop closure attempts to happen, processing localization drifts occurred during the navigation.

3 Experimental Results

3.1 System Overview

The experimental system, used for the verification of the COMPRA framework, consists of a custom built quadrotor platform, as shown in Figure 5. The platform's mass

Algorithm 2: COMPRA mission workflow

```

Input: Mission Plan
Output: Object List  $\mathbb{OL} = \{\vec{0}_{3 \times 1}, p_{object1}^{\mathcal{W}}, p_{object2}^{\mathcal{W}}, \dots, p_{objectn}^{\mathcal{W}}\}$ 
Gate Calibration //  $\mathcal{W}$  frame definition
Pre-Flight checks // software and hardware ready to fly MAV
if Pre-Flight checks then
    Take-off Sequence // stabilize hover at  $p_z^m$ 
    if Take-off Sequence then
        Exploration=True // start exploration
        while Exploration do
            if object detected then
                while object in view at time instance K do
                     $\mathbb{P}_{object}^C = [\mathbb{P}_{object}^C; p_{object,K}^C]$ 
                    if  $size(\mathbb{P}_{object}^C) > 0$  then
                         $objectLocalized=True$ 
                if objectLocalized then
                     $p_{object}^{\mathcal{W}} = \mathbb{P}_{object}^C$ 
                     $\mathbb{OL} = \{\mathbb{OL}; p_{object}^{\mathcal{W}}\}$ 
                     $objectLocalized=False$ 
                if  $T_{mission}^{current} \leq T_{mission}^{reference}$  then
                     $\psi_{ref}, wp^{\mathcal{B}} = [p_x^{\mathcal{B}} + 1, p_y^{\mathcal{B}}, p_z^m]$ 
                    Breadcrumb Waypoint List  $\mathbb{BW} = [\mathbb{BW}; wp^{\mathcal{B}}\psi]$ 
                else
                     $\psi_{return}^{ref} = \psi + \pi$ 
                     $size(\mathbb{BW}) = k$ 
                     $wp^{\mathcal{B}} = \mathbb{BW}(k)$ 
                     $\mathbb{BW} \setminus \mathbb{BW}(k)$  // remove  $k$ th entry from  $\mathbb{BW}$ ,  $\setminus$  denotes relative complement operation
                    if  $\mathbb{BW} = \{\emptyset\}$  then
                        Exploration=False
                        Land // mission completed
            else
                if Hardware and Software health check

```

is approximately 3 kg with processing payload the Intel NUC - NUC10i5FNKPA processor. The 3D lidar Velodyne VLP16 PuckLite provides 3D pointclouds at 10 Hz with 360° Horizontal FOV and 30° Vertical FOV within the range of 100 m. The lidar measurements are used in the obstacle avoidance module, as well as in the localization module, combined with Inertial measurements. The single beam lidar LIDAR-Lite v3 is mounted facing towards the ground and provides relative altitude measurements. Moreover, the platform carries the RGB-D camera Intel Realsense D455 that provides RGB frames at 30 FPS with 90° Horizontal FOV and 65° Vertical FOV, as well as depth images at 30 FPS with 86° Horizontal FOV and 57° Vertical FOV, within the range of 6 m, used in the object detection and heading regulation modules. The MAV is equipped with the low-level flight controller PixHawk 2.1 Black Cube, which provides the IMU measurements. Finally, the MAV is equipped with two 10 W LED light bars in the front arms for additional illumination and one 10 W LED light bars looking downwards, and a downward-facing single-beam lidar used to measure the distance to the ground. The COMPRA software stack has been evaluated in the Ubuntu 18.04 Operating System using the Robot Operating System (ROS) Melodic version, while the modules have been implemented either C++ or Python.



Fig. 5: The aerial system utilized in the SubT field trials for evaluating the COMPRA framework.

3.2 Field Validation Results

The performance of the proposed method was evaluated in an underground tunnel located in Luleå, Sweden with a complete lack of natural and external illumination in the tunnel, as well as other corrupting magnetic fields, while small dust particles were floating around the platform. The tunnel dimensions traversed were approximately $3.5 - 4(\text{width}) \times 3(\text{height}) \times 70(\text{length})\text{m}^3$.

3.2.1 Obstacle Avoidance

In this Section we provide two evaluations, separate from the full missions, of the artificial potential field namely: 1) Following pre-defined way-points (placed in a straight line as to not assist the avoidance) through an obstructed tunnel area with multiple obstacles, and 2) Following randomly generated position and yaw set-points in the narrow tunnel area, as to stress test the avoidance. This can be seen as a general failure of navigation or localization where way-points are given inside or too close to the tunnel walls.

Both evaluations are performed at field experimentation site with onboard localization software in-the-loop. Figure 6 shows the MAV path through the tunnel and past multiple obstacles placed in the way. The experiment video can be seen at https://youtu.be/_dh6ZEwN-zA, showing the COMPRA-enabled MAV smoothly navigate through the obstructed environment. The second obstacle avoidance evaluation can be found at <https://youtu.be/07lnKeGXFv8>, which shows the MAV being given random position and yaw set-points with 10 second intervals while Figure 7 shows one such instant of the MAV being given a way-point inside the tunnel wall and maintaining a safe distance. Figure 8 shows how the safety distances, defined by the shortest range measurement from the 3D lidar (where we have removed dust hits etc. with a 3-point median filter), are maintained throughout the above mentioned experiments as well as through the full mission. The minimum distance to any point in the 3D point-cloud was 0.80m, which is well above the MAV safety-critical radius of around 0.5m (with propellers), and occurred when the MAV is commanded to move directly into an uneven part of the tunnel wall. While there is back-and-forth movements when the MAV is commanded to move directly into the wall, they do not produce overly oscillatory or unstable flight behavior of the MAV.

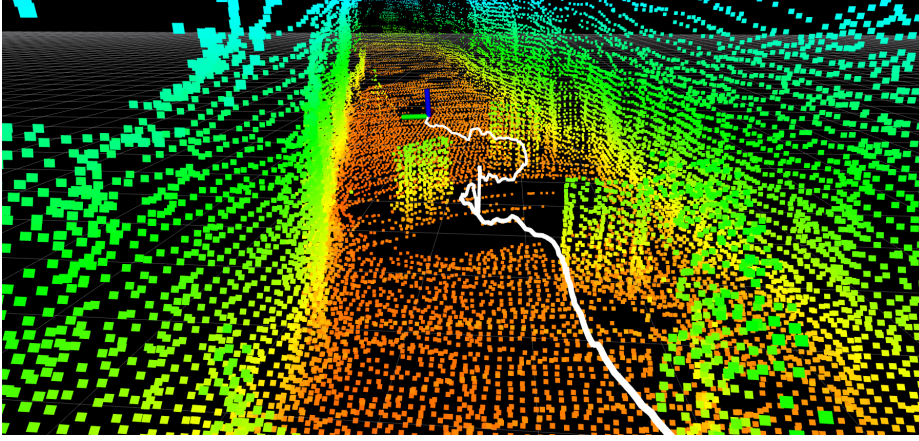


Fig. 6: Visualization of the MAV path through the obstructed tunnel section and the local pointcloud map of the environment produced by LIO_SAM.

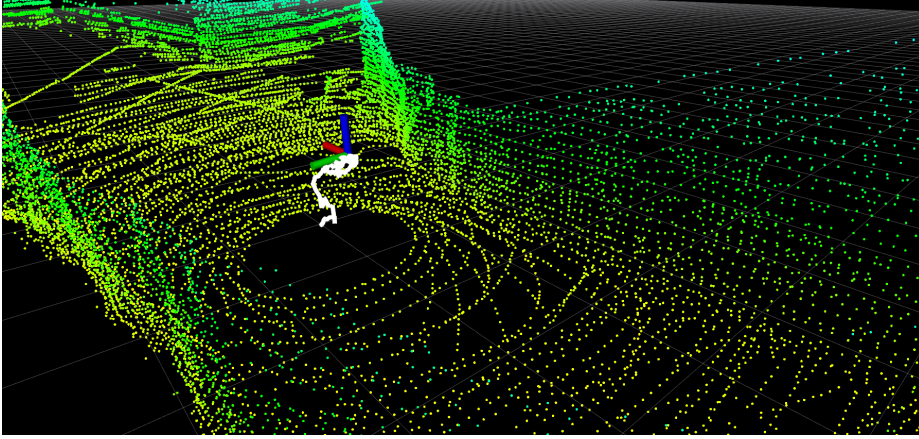


Fig. 7: Visualization of the MAV path when given a way-point 3 meters into the wall, maintaining 1m distance.

3.2.2 Full Mission

This part presents experimental results from deploying the COMPRA enabled MAV in an emulated full search and rescue mission. A video demonstrating the full mission execution can be found at <https://youtu.be/egxGgtbsyO8>.

In this scenario, a portable calibration gate consisted of a bundle of four AprilTags, placed in front of the vehicle, is used to initialize the global coordinate frame in which the objects of interest will be localized. The experiment is conducted in a curvy part of the underground environment and the objects of interest include a survivor, a helmet, a rope, a backpack, and a fire extinguisher placed to the side of the tunnel walls. The MAV was given the high level command to navigate along the tunnel for 70sec at around 0.9m/s and at a constant 0.8m height from the ground, and then return to base. The complete mission from the take-off command until after landing was handled

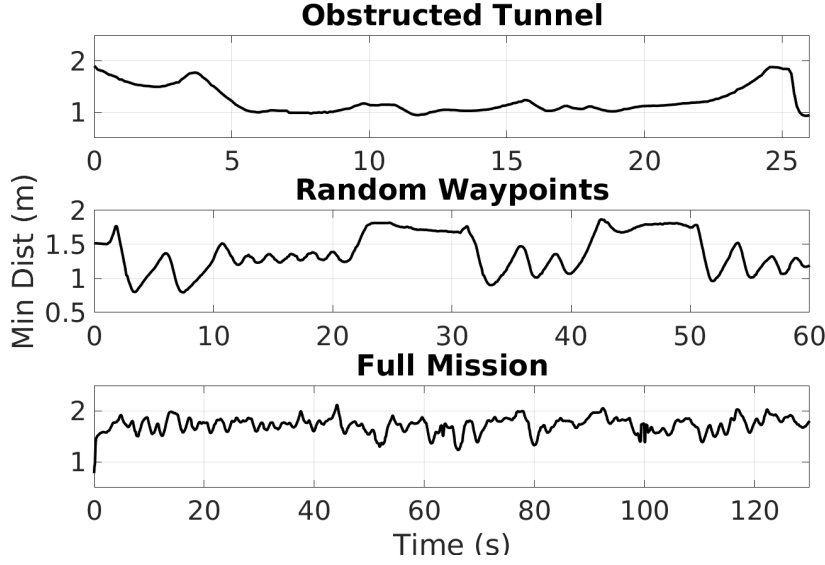


Fig. 8: The minimum-distance measurement from the 3D lidar during obstacle avoidance evaluations. Moving through a constrained environment (top), guaranteeing platform safety despite errors in waypoint generation (middle), and navigating the 3.5-4 m wide tunnel during the full mission (bottom).

fully autonomously onboard the platform. Figure 10 provides a visualization of the experimental results from the deployed system in the field. In this Figure the global map, part of the Lidar Odometry module, is only used for visualization purposes, without being directly used from the COMPRA framework. The Figure shows that the robot covered approximately 130-140 meters (with return) path, while localizing the artifacts, which are annotated in the Figure. It should be mentioned that the detector extracted correctly the bounding box of the backpack, but due to the illumination conditions and the view angle it was wrongly classified as a drill. In general, it was not feasible to quantify the precision of the localization results at the time of the experimental trials, since there was no ground truth measurements available for metric comparison. The path followed was smooth and consistent (without sudden or jerky movement), which is a major outcome from the potential field formulation. The minimum-distance lidar measurement can be seen in Figure 8, kept at around 1.2-2 m which implies the MAV is always close to the middle of the tunnel. The identified objects have not been part of the training dataset for the CNN-based detector, showing the applicability to identify object in those classes that have not been seen before. A bottleneck of the modified CNN model to run on the VPU is that it detects the object in close distances, while missing detections when the object is in view but in further distances. Nevertheless, this does not affect the performance of the overall system, since the localization part relies on the depth image stream, requiring the platform to get measurements from close distances with respect to the object for more reliable results. Figure 9 depicts snapshots from the object detection module. The detection module rate varied around 8 FPS.

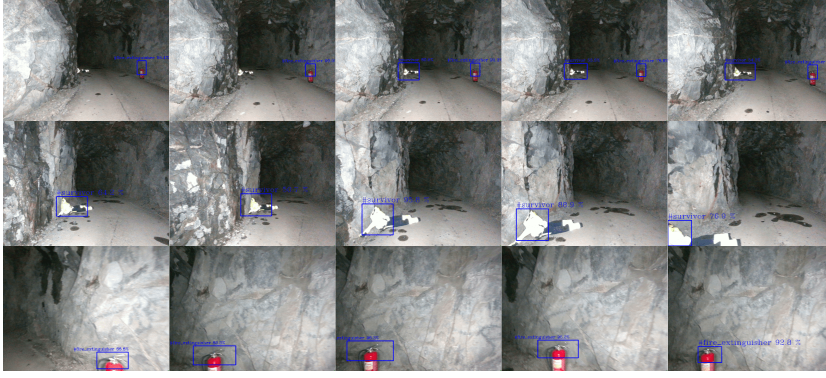


Fig. 9: Visualization of true positives from detected objects (bounding boxes and class probabilities) during the full mission.

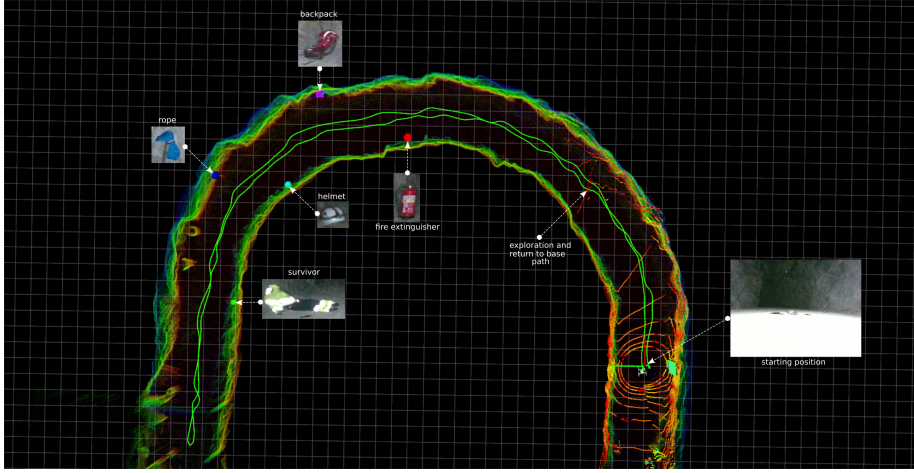


Fig. 10: Visualization of the full mission performed in an underground tunnel using the proposed framework

3.3 Discussion & Lessons Learned

During the field tests we had to address issues related to state estimation, heading regulation, artifact detection and flight time of the platform. More specifically, the underground area that the MAV explored was quite challenging with respect to the geometry and self-similar shape in terms of the Lidar-Inertial method. Overall, we tuned the Lidar-Inertial method to operate in underground environments, while we aim to enhance the methodology to support large-scale and long-term operations incorporating sensor fusion in the pipeline. A challenge in terms of obstacle avoidance is achieving the desired flight behavior both in obstacle free areas where the aim is moving as quickly as possible, and in obstacle rich areas, where stable avoidance behavior should be prioritized over speed. We aim to include adaptive schemes that match the optimal flight speed to the proximity of obstacles in the environment. The heading contour extraction main operation assumption is the combination of pitch dark environments

with the platform onboard illumination that spreads light in the walls surrounding the platform and creates the open space notion in the dark area of the tunnel. A bottleneck in this method we identified was that in some cases false positive dark areas were spotted from the camera and the heading was instantaneously erroneous. The main discussion point related to the artifact detection method was that it missed the detection of objects in longer distances and this causes non-detected objects in case the MAV does not navigate close to them (e.g ceiling). Finally, the flight time of the aerial platform is critical for the mission and game changer when designing autonomy frameworks. COMPRA assumes lightweight platforms with limited flight time, aiming for quick deployment as well as fast navigation and scouting behaviour of unexplored areas, instead of detailed area coverage.

4 Conclusions

This work presented COMPRA navigation framework for MAVs, targeting search-and-rescue operations in subterranean environments. The COMPRA framework enables the fast deployment of a fully autonomous MAV to navigate along previously unknown tunnel areas. The proposed autonomy architecture combines 3D lidar-inertial state estimation, position based NMPC control, potential field based obstacle avoidance, heading alignment with the tunnel axis as well as object detection, localization and mission behaviour. COMPRA's main aim is to keep the overall system compact, reactive, resilient, and with low complexity as a baseline solution for a complete SubT exploration and object localization mission. Multiple field trials successfully demonstrate the performance and efficacy of the method towards real-life applications in realistic subterranean tunnels.

Declarations

Funding: This work has been partially funded by the European Unions Horizon 2020 Research and Innovation Programme under the Grant Agreement No. 869379 illumination.

Conflict of interest: The authors have no conflicts of interest with any related parties.

Competing Interests: Not applicable

Availability of data and material: ROSbags of sensor and submodule output data from field experiments can be made available at the suggestion of the reviewers and editors.

Authors' Contributions: Björn Lindqvist and Christoforos Kanellakis: Development, implementation, system integration and field work, relating to all presented submodules and developments. Main manuscript contributors. Sina Sharif Mansouri: Software development and field expertise. Ali-akbar Agha-mohammadi: Advisory, development lead for Team CoSTAR in DARPA SubT Challenge. George Nikolakopoulos: Advisory, manuscript contributions, head of Luleå University of Technology Robotics&AI Team. All authors have read and approved the manuscript

Ethics approval: Not applicable.

Consent to Participate: Not applicable.

Consent to Publish: All authors comply with the consent to publish.

Acknowledgements This work has been partially funded by the European Unions Horizon 2020 Research and Innovation Programme under the Grant Agreement No. 869379 illuminate.

References

1. A. Kalantari, T. Touma, L. Kim, R. Jitosho, K. Strickland, B.T. Lopez, A.A. Agha-Mohammadi, in *2020 IEEE Aerospace Conference* (IEEE, 2020), pp. 1–10
2. D. Thakur, G. Loianno, W. Liu, V. Kumar, in *International Symposium on Experimental Robotics* (Springer, 2018), pp. 191–200
3. S.S. Mansouri, C. Kanellakis, E. Fresk, D. Kominiak, G. Nikolakopoulos, *Control Engineering Practice* **74**, 118 (2018)
4. J.G. Rogers, R.E. Sherrill, A. Schang, S.L. Meadows, E.P. Cox, B. Byrne, D.G. Baran, J.W. Curtis, K.M. Brink, in *Ground/Air Multisensor Interoperability, Integration, and Networking for Persistent ISR VIII*, vol. 10190 (International Society for Optics and Photonics, 2017), vol. 10190, p. 1019017
5. DARPA. Subterranean challenge (SubT). URL <https://www.subtchallenge.com/>
6. TEAM COSTAR. NeBula autonomy. URL <https://costar.jpl.nasa.gov/>
7. T. Dang, F. Mascarich, S. Khattak, H. Nguyen, H. Nguyen, S. Hirsh, R. Reinhart, C. Papachristos, K. Alexis, in *2020 IEEE Aerospace Conference* (IEEE, 2020), pp. 1–8
8. M. Petrлік, T. Báča, D. Heřt, M. Vrba, T. Krajník, M. Saska, *IEEE Robotics and Automation Letters* **5**(2), 2169 (2020)
9. J. Sandino, F. Vanegas, F. Maire, P. Caccetta, C. Sanderson, F. Gonzalez, *Remote Sensing* **12**(20), 3386 (2020)
10. T. Özaslan, G. Loianno, J. Keller, C.J. Taylor, V. Kumar, J.M. Wozencraft, T. Hood, *IEEE Robotics and Automation Letters* **2**(3), 1740 (2017)
11. S.S. Mansouri, C. Kanellakis, D. Kominiak, G. Nikolakopoulos, *Robotics and Autonomous Systems* **126**, 103472 (2020)
12. M. Kamel, T. Stastny, K. Alexis, R. Siegwart, in *Robot operating system (ROS)* (Springer, 2017), pp. 3–39
13. S. Khattak, C. Papachristos, K. Alexis, *Journal of Field Robotics* **37**(4), 552 (2020)
14. T. Dang, F. Mascarich, S. Khattak, H. Nguyen, N. Khedekar, C. Papachristos, K. Alexis, *Field and Service Robotics (FSR)* (2019)
15. T. Dang, F. Mascarich, S. Khattak, C. Papachristos, K. Alexis, in *2019 IEEE/RSJ International Conference on Intelligent Robots and Systems (IROS)* (IEEE, 2019), pp. 3105–3112
16. S. Kohlbrecher, O. Von Stryk, J. Meyer, U. Klingauf, in *2011 IEEE international symposium on safety, security, and rescue robotics* (IEEE, 2011), pp. 155–160
17. L. Meier, D. Honegger, M. Pollefeys, in *2015 IEEE international conference on robotics and automation (ICRA)* (IEEE, 2015), pp. 6235–6240
18. T. Lee, M. Leok, N.H. McClamroch, *Asian Journal of Control* **15**(2), 391 (2013)
19. D. Mellinger, V. Kumar, in *2011 IEEE international conference on robotics and automation* (IEEE, 2011), pp. 2520–2525
20. C. Kanellakis, S.S. Mansouri, G. Georgoulas, G. Nikolakopoulos, in *International Conference on Robotics in Alpe-Adria Danube Region* (Springer, 2018), pp. 173–180
21. B. Lindqvist, S.S. Mansouri, A.a. Agha-mohammadi, G. Nikolakopoulos, *IEEE Robotics and Automation Letters* **5**(4), 6001 (2020)
22. E. Small, P. Sopasakis, E. Fresk, P. Patrinos, G. Nikolakopoulos, in *2019 18th European Control Conference (ECC)* (2019), pp. 3556–3563
23. T. Shan, B. Englot, D. Meyers, W. Wang, C. Ratti, D. Rus, in *IEEE/RSJ International Conference on Intelligent Robots and Systems (IROS)* (2020)
24. S.S. Mansouri, M. Castano, C. Kanellakis, G. Nikolakopoulos, in *12th International Conference on Computer Vision Systems (ICVS)* (2019, to appear)
25. P. Sopasakis, E. Fresk, P. Patrinos, arXiv preprint arXiv:2003.00292 (2020)
26. B. Hermans, P. Patrinos, G. Pipeleers, *IFAC-PapersOnLine* **51**(20), 234 (2018)
27. C.W. Warren, in *1989 IEEE International Conference on Robotics and Automation* (IEEE Computer Society, 1989), pp. 316–317
28. N. Otsu, *IEEE transactions on systems, man, and cybernetics* **9**(1), 62 (1979)

-
29. E.W. Weisstein, From MathWorld—A Wolfram Web Resource. <http://mathworld.wolfram.com/MooreNeighborhood.html> (2005)
 30. Intel. OpenVINO™ Toolkit. URL <https://docs.openvino toolkit.org/latest/index.html>
 31. A. Bochkovskiy, C.Y. Wang, H.Y.M. Liao, arXiv preprint arXiv:2004.10934 (2020)